

Local microbubble concentration by defocused volumetric shadowgraphy with a single camera

Cornel, Wout; Westerweel, Jerry; Poelma, Christian

DOI

[10.3929/ethz-b-000279233](https://doi.org/10.3929/ethz-b-000279233)

Publication date

2018

Document Version

Final published version

Published in

Proceedings 18th International Symposium on Flow Visualization

Citation (APA)

Cornel, W., Westerweel, J., & Poelma, C. (2018). Local microbubble concentration by defocused volumetric shadowgraphy with a single camera. In T. Rösgen (Ed.), *Proceedings 18th International Symposium on Flow Visualization* ETH Zürich. <https://doi.org/10.3929/ethz-b-000279233>

Important note

To cite this publication, please use the final published version (if applicable). Please check the document version above.

Copyright

Other than for strictly personal use, it is not permitted to download, forward or distribute the text or part of it, without the consent of the author(s) and/or copyright holder(s), unless the work is under an open content license such as Creative Commons.

Takedown policy

Please contact us and provide details if you believe this document breaches copyrights. We will remove access to the work immediately and investigate your claim.



LOCAL MICROBUBBLE CONCENTRATION BY DEFOCUSED VOLUMETRIC SHADOWGRAPHY WITH A SINGLE CAMERA

W.A. Cornel^{1,c}, J. Westerweel¹, C. Poelma¹

¹Department of Process and Energy, Delft University of Technology, 2628 CA Delft, The Netherlands
^cCorresponding author: Tel.: +31152784194; Email: w.a.cornel@tudelft.nl

KEYWORDS:

Main subjects: local bubble concentration, defocused volumetric shadowgraphy, microbubbles

Fluid: two-phase, flow induced by rising gas bubbles

Visualization method: defocused shadowgraphy imaging

Other keywords: local void fraction, single camera, imaging

ABSTRACT: *The challenge presented in this research is to determine the local volumetric bubble concentration (or void fraction) in the center of a microbubble cloud with limited optical access and without disturbing the flow. By applying defocused volumetric shadowgraphy to an aerated water column we were able to measure the characteristics of single microbubbles in the control volume for a void fraction of 0.078 percent. The time-averaged local bubble concentration in the center of the water column was measured over four periods (800 seconds each) to investigate the repeatability. Two reference methods, based on differential pressure ($\Phi_V = 0.081$ percent ± 0.011) and direct observation of the bubble's in-depth z -position, both validate the results independently.*

1 Introduction

The presence of microbubbles in fluids has considerable effects on the liquid compressibility and thus the speed of sound, even for moderate volume fractions. Microbubbles are small compressible gas bubbles with typical diameters between 1 μm and 1 mm. Knowledge the local volumetric bubble contraction (or void fraction) is of key importance in several industrial processes, such as the production of ammonia and water waste treatment [1]. Especially for industrial processes exposed to high pressures or temperatures, such as fuel injectors, access to the region of interest in the flow can be difficult. Furthermore, the flow phenomena of interest might be locally disturbed by the presence of intrusive measurement sensors.

Direct imaging methods are non-intrusive, have the ability to characterise particle shape in great detail and are relatively inexpensive [2-3]. Shadowgraphy or backlighting has the advantages offered by digital imaging methods such as visualization of objects in high spatial resolution, identification of particle images and extraction of their characteristics [4]. Also, this measurement method is robust for bubbles as no random dust particles are picked up [1]. In fact, the main disadvantage of shadowgraphy is the loss of depth information when objects are projected on a two-dimensional image. Therefore, many of the proposed imaging techniques for volumetric measurements use multiple cameras to construct a three-dimensional space. However, some articles in literature report imaging techniques for 3D particle positioning based on a *single* camera. Combining shadowgraphy with defocused imaging enables the acquisition of depth information by the degree of out-of-focus from a single camera. Using this principle, the distance from the focus plane is derived from determining the image intensity gradient, or blurriness, over the bubbles' edges. The idea of using focal gradients to infer depth from images was introduced by Pentland in 1987 [5]. He examined the focal gradients resulting from the

limited depth of field inherent in optical systems as a useful source of depth information. By measuring the error in focus (i.e. focal gradient) the depth in the image can be estimated [5].

In recent years many researchers elaborated on defocused shadowgraphy imaging to determine locations and sizes for synthetic particles [6-8], larger gas bubbles [9] and dense sprays [3][10-14]. Lebrun et al (1993) used two CCD cameras with the same angle of view to deduce particle diameters from the image contrast and the cross-section areas of the defocused images. More recently, Bröder and Sommerfeld (2007) developed an interesting planar defocusing imaging technique for the analysis of the hydrodynamics in bubbly flows based on intensity gradients to define the depth of field of the imaging plane for bubble diameters between 2.0 and 4.0 mm. The intensity gradient over the boundary of the microbubble in the image, or blurriness, contains information on the in-field depth position z relative to the object focal plane. Fdida et al. (2010) used the calibration of the point spread function (PSF) to determine the drop size distribution by counting drops. Malot and Blaisot (2000) developed an imaging model based on the point spread function to determine the drop size distributions of sprays produced by low-velocity plain cylindrical jets. Wavelet transforms, based on the point spread functions, have been constructed to perform hologram analysis [4][12]. The study of Ren et al. (1996) shows that corrections for the estimated diameters are less significant for larger particles. Digital pattern recognition algorithms deliver accurate and robust results as the projected particles are close to circular. Lee et al. (2009) developed a modified in-focus parameter based upon optical principles to identify particles. Their adaptive sampling volume methodology varies with each particle size based upon a critical in-focus value [2]. By linking particle depth location to the circle of confusion (COC), determined from the gray scale gradients of the 2D image profile and from image contrast considerations, Legrand et al. (2016) obtained less than 20 percent error in particle sizing with displacements up to 30 particle diameters away from the focus plane [3].

Closely related to defocused volumetric imaging is defocused digital particle image velocimetry (DDPIV) where flow fields of tracer particles are measured [15]. For example, Willert and Gharib (1992) proposed a new approach to track particles in space and time by using defocusing and an embedded mask in the camera lens to observe triangular patterns [6]. De Haeck et al (2009) proposed an alternative method to locate depth from 2D-images combines backlighting and glare point velocimetry [1]. Only bubbles inside the thin laser sheet have two symmetrical glare points, so that the control volume is well-defined. The laser sheet needs to be perpendicular to the optical access, which makes this method unsuitable for cases with limited optical access.

In this research we further elaborate on defocused volumetric shadowgraphy by extending it to smaller compressible gas microbubbles with a mean diameter in the order of 600 μm and apply Circular Hough Transform (CHT) and Sobel edge detection for bubble shape recognition. The objective of this paper is to propose a method, based on intensity gradients, to measure bubble concentrations in aerated liquids locally from images captured by one single camera. As smaller droplets and dense sprays (typically particle size $< 100 \mu\text{m}$) and larger bubbles (with typical diameters $> 2.0 \text{ mm}$) have been studied extensively over recent years, only limited literature is publicly available for microbubbles with diameters smaller than 1 millimeter. These microbubbles have the advantages of having a relative large surface to volume and approximate sphericity which allows for precise volumetric determination. We employ defocused volumetric shadowgraphy to acquire bubble size distribution and locations accurately. The bubble z -position is relative to the focus plane and thus the measurement volume is

well-defined. On the other hand, the *sign* of the relative distance from the focus plane cannot be traced back from the images. Therefore, it is possible to determine precisely if bubbles are located within a specified control volume, only we do not know whether the bubbles are in front or behind the focus plane [3]. A second advantage of defocused imaging is the ability to measure bubble characteristics, such as volume, since the selected gas bubbles have sharp contours in the focus plane.

The outline of this paper is as follows: The next section describes the imaging model and point spread function which approaches the defocused intensity profile of the image. From this, the experimental setup, methodology and calibration procedure are described. The result section discusses the measured bubble concentrations for the center of a bubble cloud and two validation techniques. The last section concludes the results and provides an outlook for future work.

2 Imaging model

An optical imaging systems with backlight configuration is used in this research (see figure 1). The intensity distribution in the image is the convolution of the point spread function (PSF), i.e. the system response, and the object function [7]. Pentland (1987) showed that the shape of the PSF can be approximated by a Gaussian function for non-coherent polychromatic light and that the PSF depends on the relative distance between the focus plane and the object [5][14]. The Gaussian function flattens out for particles further located away from the focus plane, i.e. the object projection of the image plane becomes increasingly blurred. Consequently, the intensity gradient of the edge between the projected object and the background decreases too. The contribution of non-spherical aberrations is assumed to be negligible by imposing the PSF to have a generic symmetrical Gaussian shape [10].

3 Bubble shape

The degree of bubble sphericity depends on the dimensionless Eötvös (or Bond) number, Morton number Mo and the Reynolds number and the regions are indicated by the Grace diagram. The Eötvös number compares the gravitational force ($\rho g L^3$) with the surface force (σL), while the Reynolds number is the ratio of inertia to viscous forces. The Morton number ($g \mu^4 / \rho \sigma^3$) follows from a dimensional analysis by Rosenberg (1950) on the motion of air bubbles in liquids. Chesters (1975) reformulated the Morton number as $We^3 / (Re^4 Fr^2)$, where the Weber number describes the ratio of inertia to surface forces and the Froude number Fr is the ratio of inertia to gravity. Microbubbles with typical diameters of 600 μm in water (depth ≈ 0.5 m) under standard conditions approach sphericity as the surface tension dominates over the gravitational force. For these dimensionless numbers the Grace diagram indicates that bubbles are located far into the spherical regime. Sphericity is an important bubble characteristic that enables us to expand the projected two-dimensional bubble into the three-dimensional space accurately. Especially for larger gas bubbles, which may become irregular wobbling as the relative influence of the surface tension lowers, determining the volume from projected images may become more challenging.

4 Experimental facility and methods

In this work, defocused shadowgraphy imaging is used to estimate the depth of objects in single 2D-images captured by one single camera. Basically, the object $\{x, y\}$ -coordinates are directly available by processing correctly calibrated single 2D-images, while the z -coordinates follows from the amount of defocusing or blurring.

An experimental setup has been built to generate an aerated liquid (see figure 1). A static water column with a height of 1.30 meter, filled with filtered tap water, has optical access provided by two opposing windows, where the camera optical axis is aligned with a LED panel for diffuse incoherent backlight illumination. Two fine-pore aerators (Pentair) are installed at the bottom of the water column and generate adjustable gas bubble clouds with bubble diameters between roughly 500 and 900 micrometers. Thus, typical particle sizes are much larger than the wavelength of the incoherent light (i.e. $D/\lambda \gg 1$). Two reference measurement methods are added to validate the observed depth position by the single camera. First, a reference camera is installed, perpendicular to the optical axis of the main camera, to validate the bubble position in the $\{y, z\}$ -plane. In this way, the z -coordinate is observed directly. Secondly, the void fraction is measured globally by the pressure difference over the aerated liquid and a reference water column.

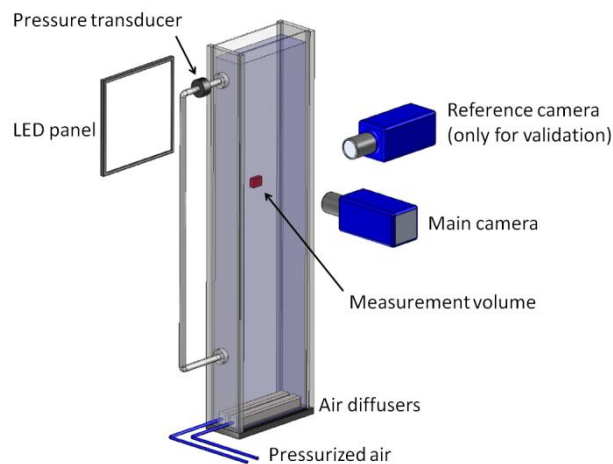


Fig. 1. Systematic overview of experimental setup (not to scale). The measurement volume (red rectangular) is aligned between the centerline of the LED panel and the main camera. Two air diffusers ($300 \times 40 \times 40 \text{ mm}^3$) are installed at the bottom and connected to pressurized air. The differential pressure transducer and the reference camera serve as reference methods.

The point spread function (PSF) describes the complete, quantitative response of the optical system [14]. The response is determined experimentally by attached bubbles on the calibration sheet. The calibration is performed by recording multiple images of a calibration sheet, with attached microbubbles and spacing markers, by translating the CCD camera (LaVision Imager Intense), equipped with a 105 mm objective (Nikkor), in steps between $50 \mu\text{m}$ (near the object focal plane) and $400 \mu\text{m}$ (further away). The aperture of the objective is set to 4 to obtain a small depth of field. The 12-bit grey level frame images have a resolution of 1040 by 1376 pixels. For each image the magnitude of the intensity gradient of the attached bubble is measured to construct a calibration curve, which relates the magnitude of the image intensity gradient and distance from the focal plane (see figure 4).

Once the imaging system is calibrated and the calibration sheet is removed, a bubble cloud of approximately $110 \times 300 \text{ mm}^2$ in cross-section is generated when releasing compressed air through the fine-pore aerators at the bottom of the water column. Contrary to the calibration procedure, the unbounded bubbles are moving towards the free surface. Motion blur, the effect that moving objects are smeared out over their trajectory path, might cause blurred edges too. In order to reduce motion blur in the image, the exposure time is set to $50 \mu\text{s}$ during the entire experiment. The image pixel resolution is 0.01086 mm/pixel , corresponding to a field of view of 14.9 mm by 11.3 mm . Assuming an

average bubble rising velocity of 100 mm/s, the travelled distance during exposure of the camera is 5.0 μm , or 0.5 pixels. The control volume has dimensions of $10 \times 8 \times 5 \text{ mm}^3$ (L \times W \times H) and centered in the middle of the bubble cloud (see figure 1). During the experiments the camera and lens settings (i.e. aperture, focal length, exposure time) are constant and the frame rate is set to 0.5 Hz.

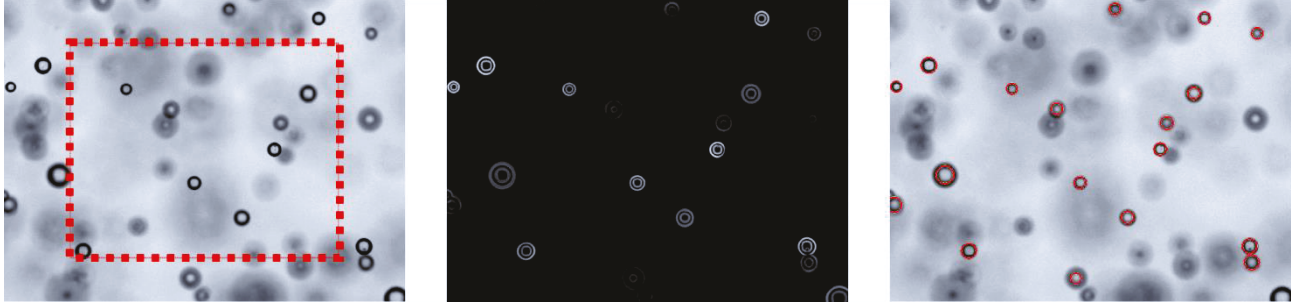


Fig. 2. Unprocessed image with projected control volume (left), magnitude of the intensity gradient (center) and detected bubbles (right) for the same image. The center image is used for detecting the $\{x, y\}$ -coordinates of the bubble center.

In principle the microbubble detection procedure is based on the Circular Hough Transform (CHT) and Sobel edge detection from the MATLAB image processing toolbox, in combination with own modifications. First, the recorded raw images from the camera are smoothed by a Gaussian filter to remove the high spatial frequency originated from the stochastic nature of incoming photons at the camera sensor. Optimizing of the raw image has the advantage of uncovering the intensity profile of the bubbles freed from background noise. The PSF is determined experimentally from the intensity gradients in the filtered image. To further improve the robustness of the proposed method, the intensity gradient is determined over four directions and the median is used to determine the out-of-focus distance. This additional robustness step ensures that no single outlier causes incorrect values. Also, the direction of the gradient is used to separate the inner and outer edge of the dark circle. As both the calibration and measurements are processed with the same procedure, the intensity gradients are matched and consequently the depth position can be obtained from the calibration.

This intensity gradient-based method does not require thresholding to identify objects, because the intensity gradient is directly related to the out-of-focus distance to the focus plane. However, too much defocused microbubbles are blurred to high extent and extracting their characteristics becomes increasingly difficult. Therefore, only sharp-contoured bubbles positioned closely to the focus plane are considered in this work. The sensitivity of the CHT is set to be able to detect bubbles at an absolute distance of at least 4 mm from the focus plane. To avoid missing bubbles at the edge of the control volume due to not being recognized by the CHT, the control volume has an absolute depth distance of 2.5 mm, to ensure that all qualified bubbles are detected. Individual bubble volumes are estimated by the equivalent spherical bubble diameter, where the bubble radius is the distance from the identified bubble center to the median of the four maximum edge intensity gradients. In the final step of the image processing procedure void fractions Φ_V are calculated per image by summing up the volumes of single bubbles and divide them over the control volume. The total average void fraction $\langle \Phi_V \rangle$ is the average of the void fractions per image.

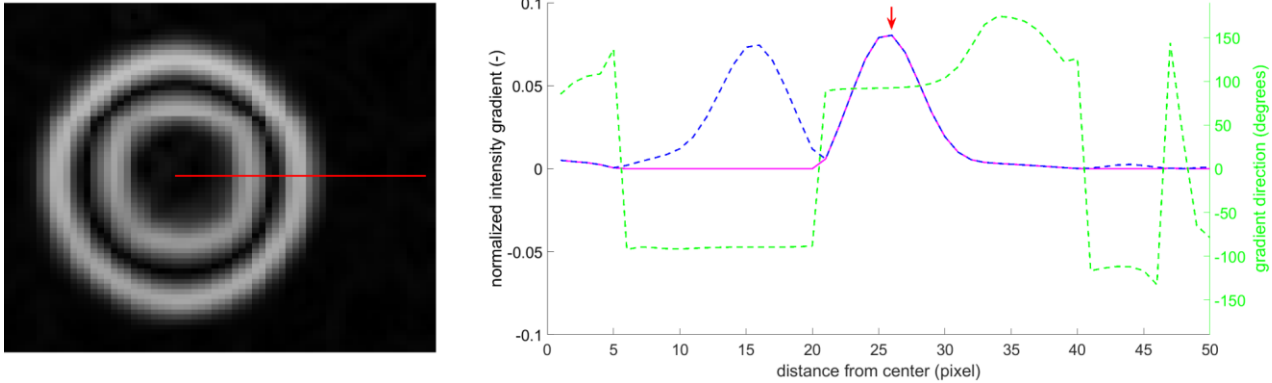


Fig. 3. Left: the red line represents one of the four intensity profiles over the edge of the bubble. Right: the direction of the gradient (dotted green line) ensures that the outer circle is selected by zeroing the intensity gradient for negative angles (mage

5 Differential pressure reference measurement

A reference differential pressure measurement is performed in order to validate the measured bubble concentration in the control volume. The injected bubbles lower the effective density and thus reducing the hydrostatic pressure (see figure 1). Even though the bubble concentrations are low ($\Phi_V \ll 1$ percent), the differential pressure sensor is able to measure accurately the pressure difference between the single-phase and aerated water column. The pressure drop over the test section consists of the static head and the wall friction [16]. The latter depends on the Reynolds number. For the single-phase case the water is stagnant, while the induced liquid velocity by the rising gas bubbles is assumed to be negligible. Therefore, the effect of the main contribution of the pressure difference for aerated liquids is:

$$\Delta P = \underbrace{\rho_g \Phi_V g H + \rho_l (1 - \Phi_V) g H}_{\text{aerated liquid}} - \underbrace{\rho_l g H}_{\text{reference}} \rightarrow \Phi_V = \frac{\Delta P}{g H (\rho_g - \rho_l)} \quad (1)$$

where ρ_g and ρ_l are the gas and liquid densities respectively, H the height of the test section and g the gravitational acceleration. Pressure differences are only measurable for substances with different densities. Considering that $\rho_g \ll \rho_l$, equation (1) approximates $\Phi_V \approx -\Delta P / (\rho_l g H)$. The accuracy of the Validyne DP45 very low pressure transducer is ± 0.5 percent over the full range. Typical pressure differences are in the range of 10 to 150 Pa, so that the membrane with the maximum pressure of 550 kPa was selected. This corresponds to an absolute measurement uncertainty of 5.5 Pa, or approximately 0.55 mm water column. This uncertainty corresponds to an error of 0.056 percent volume fraction for the microbubbles (based on equation 1). Because the sensitivity of the pressure transducer, the pressure difference is measured at a temporal frequency of 1 kHz over 30 seconds to reduce pressure fluctuations below the measurement accuracy [16].

6 Results

6.1 Calibration curve

The normalized intensity gradient of one bubble with diameter of $950\ \mu\text{m}$, attached to the calibration sheet, is fitted with a function of the summation of three Gaussian terms. Clearly, the calibration curve is not symmetrical (see figure 4). The skewness, a measure of the asymmetry of the data around the mean, is positive ($+1.3403$) and indicates that the data to the left of the calibration curve are spread out more than to the right. This observation is in agreement with the findings of Fdida et al. (2010), who referred to the asymmetry as the ‘perspective effect’. An alternative method to describe the function shape is the kurtosis, which measures the tailedness of the calibration curve. The calculated kurtosis of 3.61 exceeds the kurtosis of a univariate normal distribution (3.00), meaning that the calibration curve is more peaked than the univariate normal distribution.

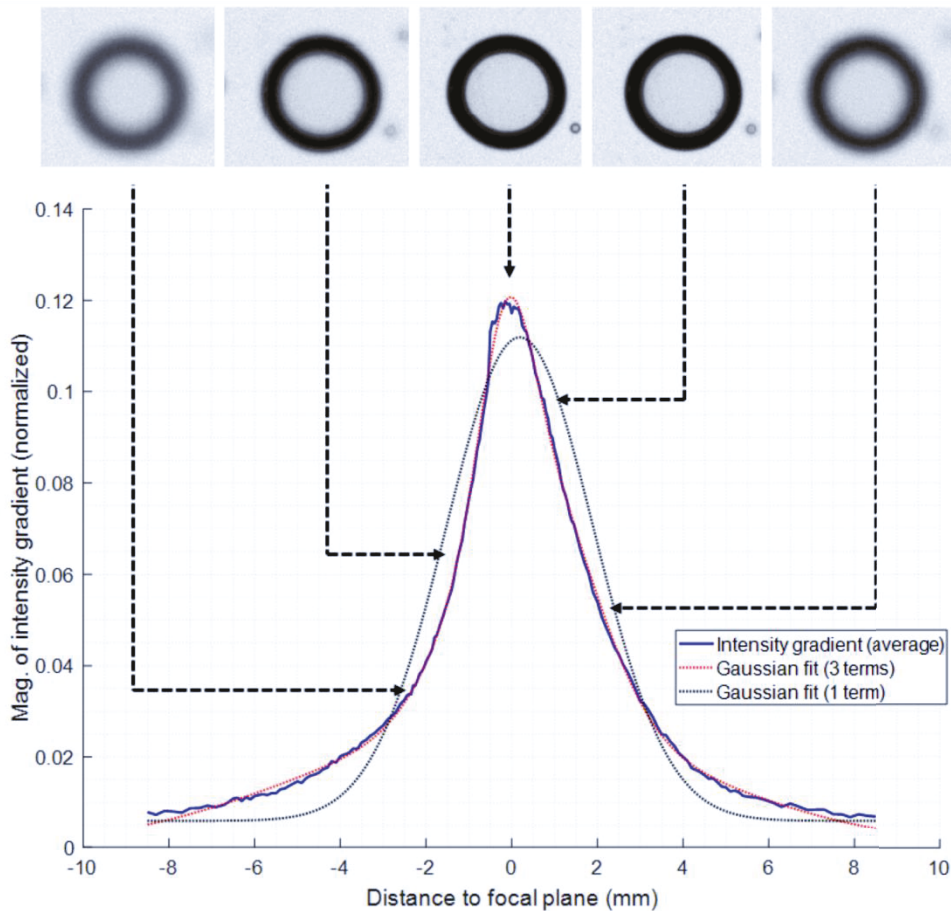


Fig. 4. Calibration curve of the defocused distance to object focal plane (bottom) with examples of defocused calibration bubbles (top)

6.2 Local bubble concentrations in bubble clouds

The void fraction in the center of the microbubble cloud is determined at $400\ \text{mm}$ below the free surface. In total, $4\ 524$ microbubbles were detected within the control volume over $1\ 600$ consecutive images.

In order to further inspect the robustness of the recognition method, detected bubbles are marked and visually inspected whether the particle indeed are classified correctly. Table (1) presents the measured void fraction in time periods to check for compliance with the steady-state condition. The distribution of the bubble diameters is also shown in figure (5).

Table 1: Measured bubble characteristics for four consecutive time periods of 800 seconds (i.e. 400 images) each. The bubble concentration, mean and median bubble diameter, and number of detected bubbles are stationary in time.

time period (s)	0 – 800	802 – 1600	1602 – 2400	2402 – 3200	total
bubble concentration (%)	0.079	0.076	0.076	0.079	0.078
mean diameter (mm)	0.563	0.559	0.563	0.566	0.563
median diameter (mm)	0.532	0.532	0.532	0.543	0.532
number of bubbles (-)	1164	1150	1109	1101	4524

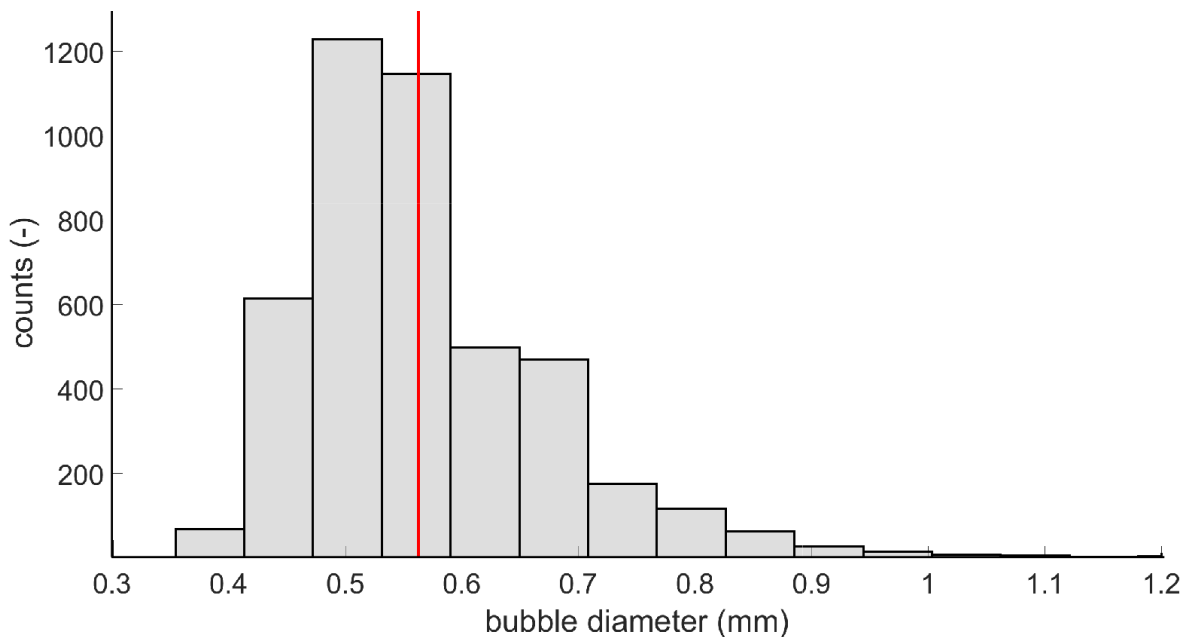


Fig. 5. Histogram of the bubble diameters based on 4 524 bubbles with average bubble size of 563 micrometer (redline)

Once the $\{x, y, z\}$ -coordinates of the microbubbles are measured accurately, bubbles that are located within the defined measurement section are selected for further analysis. Although the boundaries of the measurement volume are demarcated accurately, only the absolute z -position relative to the focus plane is known. In other words, we do not have information if the defocused bubble image is located in front or behind the focus plane. Unless all bubbles are known to be located on one side of the focus plane, no full 3D spatial representation can be reconstructed with this method. To overcome this problem, Legrand et al. [3] arbitrarily depicted the z -coordinate of the particle as positive to be able to

construct a 3D visualization. In this work we do not follow this convention, as the visualisation gives twice as high bubble concentration when the negative z -positions are mirrored in the $\{x, y, z = 0\}$ -plane.

6.3 Comparison of the z -position with reference camera

To validate the z -position found by our method we installed a reference camera, aligned with the centerline of the control volume and perpendicular to the optical axis of the main camera. Arrays of bubbles were injected now and recorded simultaneously in the measurement section by both cameras. Images from the main camera span the $\{x, y\}$ -plane, and thus need first to be processed to obtain the z -coordinate. Meanwhile, images recorded of the reference camera span the $\{y, z\}$ -plane, and hence the z -coordinate is directly observable. Using this depth-information from the second reference camera, the exact z -position can be retrieved from the intensity gradient method. Figure (6) shows the comparison with the second reference camera and validates that defocused imaging allows for determining the depth z -position of microbubbles from the recorded images by only the main camera. The offset for the z -position by the reference camera was set afterwards during processing as it proved to be very difficult to place the calibration target exactly in the focus plane of the main camera. A simple linear regression analysis is performed to test the goodness of defocused shadowgraphy for determining bubble positions (indicated by the red line). Based on the R-squared of 0.9883, the calculated z -positions has very high explanatory power.

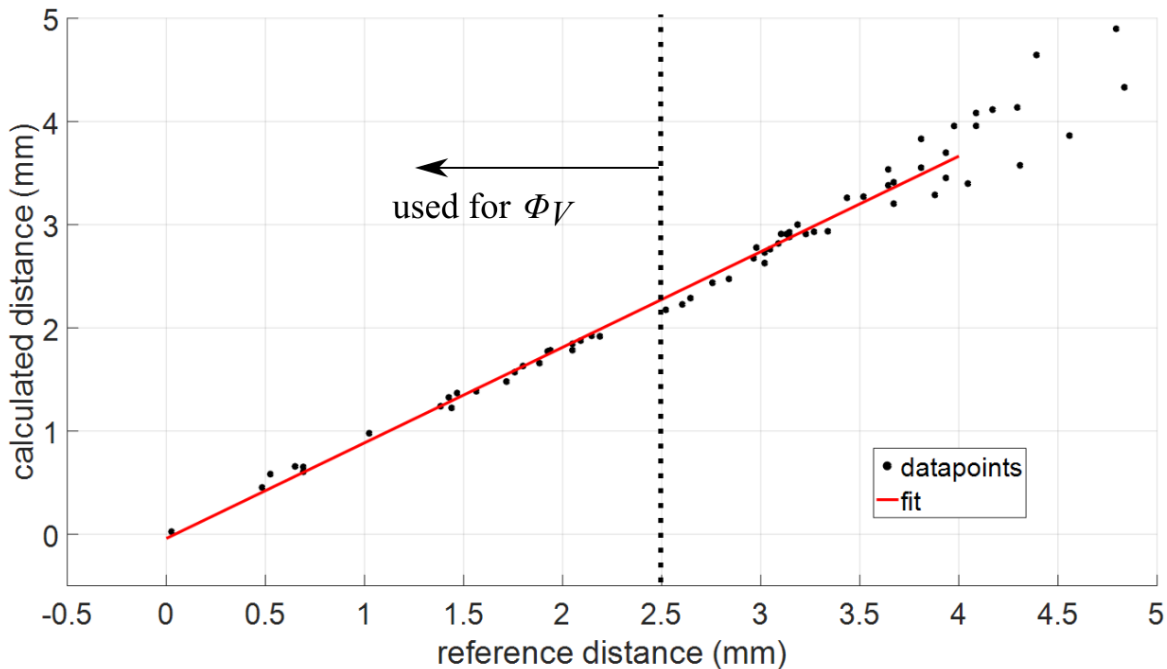


Fig. 6. Validation of the in-depth z -position with the second reference camera (horizontal axis) and the measured in-depth position by the main camera (vertical axis).

6.4 Comparison with differential pressure reference measurement

A second reference method, based on the differential pressure between two interconnected water columns, is performed to validate the correctness of the void fraction measurement. One water column is filled with single-phase liquid, while the second column (in which the measurement section is located) is aerated with gas bubbles. The reference void fraction measured by pressure difference between the single-phase water column and the aerated column equals to 0.081 ± 0.011 percent. The reference differential pressure measurement works independently from the defocused shadowgraphy in the sense that different measurement techniques are employed. However, one important limitation of the pressure difference method is the global scope, by which it is not possible to obtain local void fractions. Bubbles near the bottom of the water column experience a larger static head pressure and will be more compressed. Naturally, bubbles close to the free surface are relatively more expanded. Considering a water column of 0.95 meter, the static head compresses microbubbles at the bottom by roughly nine percent in volume and 2.9 percent in diameter, assuming isothermal compression and atmospheric pressure at the free surface. As the measurement section for defocused imaging is located near the middle of the water column (0.40 m below the free surface), the camera records bubbles with average bubble diameters and thus volume changes may be ignored. Even though the global scope of the differential pressure measurement is not able to provide local information at the control volume, yet the reference void fraction corresponds reasonable well to the obtained bubble concentration of 0.078 percent by the defocused volumetric shadowgraphy method.

7 Conclusion and Outlook

Defocused volumetric shadowgraphy is used to determine accurately the microbubble position z from 2D-images, recorded by a single camera, and provides detailed volumetric information about the number and volume of gas microbubbles in the center of a bubble cloud. It is demonstrated that this method is able to accurately determine local voids fraction for bubble clouds in (industrial) setups with limited optical access in a non-intrusive and non-disturbing manner. The bubble size distribution is determined by finding the center of the bubble using Circular Hough Transform (CHT) and Sobel edge detection from the Matlab toolbox and the radius by the median of four maximum intensity gradients. Based on the Eötvös and Bond number, the gas bubbles are considered to be spherical so that the 2D projected surface provides accurate representation for the 3D-volume. Currently, most work has been done on the density measurement of droplets in dense sprays. This work extends the literature on the field of defocused imaging and local gas fraction measurements by applying this method to detect microbubbles in liquids. In ongoing work, we extend the number of local measurements by positioning the control volume systematically throughout the fluid section to construct full bubble concentration maps for several gas flow.

8 Acknowledgement

This work is part of the public-private research programme Sloshing of Liquefied Natural Gas (SLING). The support by the Netherlands Organisation for Scientific Research (NWO) Domain Applied and Engineering Sciences, and project partners is gratefully acknowledged.

9 References

- [1] Dehaeck S, Van Parys H and Hubin A. Laser marked shadowgraphy: a novel optical planar technique for the study of microbubbles and droplets. *Experiments in Fluids*, Vol. 47, pp 333-341, 2009.
- [2] Lee C, Wu CH and Hoopes JA. Simultaneous particle size and concentration measurements using a back-lighted particle imaging system. *Flow Measurement and Instrumentation*, Vol. 20, pp 189-199, 2009.
- [3] Legrand M, Nogueira J and Lecuona A and Hernando A. Single camera volumetric shadowgraphy system for simultaneous droplet sizing and depth location, including empirical determination of the effective optical aperture, *Experimental Thermal and Fluid Science*, Vol. 76, pp 135-145, 2016.
- [4] Pu SL, Allano D, Patte-Rouland B, Malek M, Lebrun D and Cen KF. Particle field characterization by digital in-line holography: 3D location and sizing. *Experiments in Fluids*, Vol. 39, pp 1-9, 2005.
- [5] Pentland AP. A new sense for depth of field. *IEEE Transactions on Pattern Analysis and Machine Intelligence*, Vol. 9, pp 523-531, 1987.
- [6] Willert CE and Gharib M. Three-dimensional particle imaging with a single camera. *Experiments in Fluids*, Vol. 12, pp 353-358, 1992.
- [7] Lebrun D, Ozkul C, Touil CE and Blaisot JB. On-line particle size and velocity measurements by the analysis of defocused images : extended depth of field. *Proceedings of the SPIE*, Vol. 2088, pp 139-148, 1993.
- [8] Lecuona A, Sosa PA, Rodriguez PA and Zequeira RI. Volumetric characterization of dispersed two-phase flows by digital image analysis. *Measurement Science and Technology*, Vol. 11, pp 1152-1161, 2000.
- [9] Bröder D and Sommerfeld M. Planar shadow image velocimetry for the analysis of the hydrodynamics in bubbly flows. *Measurement Science and Technology*, Vol. 18, pp 2513-2528, 2007.
- [10] Blaisot J-B and Ledoux M. Simultaneous measurement of diameter and position of spherical particles in a spray by an original imaging method. *Applied Optics*, Vol. 37, pp 5137-5144, 1998.
- [11] Malot H and Blaisot J-B. Droplet size distribution and sphericity measurements of low-density sprays through image analysis. *Particle & particle system characterization*, Vol. 17, pp 146-158, 2000.
- [12] Buraga-Lefebvre C, Coëtmelec S, Lebrun D and Özkul C. Application of wavelet transform to hologram analysis: three-dimensional location of particles. *Optics and Lasers in Engineering*, Vol. 33, pp 409-421, 2000.
- [13] Blaisot J-B and Yon J. Droplet size and morphology characterization for dense sprays by image processing: application to the Diesel spray. *Experiments in Fluids*, Vol. 39, pp 977-994, 2005.
- [14] Fdida N and Blaisot J-B. Drop size distribution measured by imaging: determination of the measurement volume by the calibration of the point spread function. *Measurement Science and Technology*, Vol. 21, 2010.
- [15] Pereira F and Gharib M. Defocusing digital particle image velocimetry and the three-dimensional characterization of two-phase flows. *Measurement Science and Technology*, Vol 13, No. 5, pp 583-694, 2002.
- [16] Poelma C. Experiments in particle-laden turbulence: simultaneous particle/fluid measurements in grid-generated turbulence using particle image velocimetry. *Thesis TU Delft*, pp 49-51, 2004 .
- [17] Ren KF, Lebrun D, Özkul C, Kleitz A, Gouesbet G and Grehan G. On the measurement of particles by imaging methods: theoretical and experimental aspects. *Particle & particle system characterization*, Vol. 13, pp 156-164, 1996.

Copyright Statement

The authors confirm that they, and/or their company or institution, hold copyright on all the original material included in their paper. They also confirm they have obtained permission, from the copyright holder of any third-party material included in their paper, to publish it as part of their paper. The authors grant full permission for the publication and distribution of their paper as part of the ISFV18 proceedings or as individual off-prints from the proceedings.